Desalination and Water Treatment
www.deswater.com

doi:10.5004/dwt.2021.27340

228 (2021) 229–241
July

Evaluation of phenol removal performance in backlight cascade photocatalytic reactor using artificial neural network and random forest methods

Amir Mohammad Khaksar[a], Sara Nazif[a,*], Amir Taebi[b], Ebrahim Shahghasemi[a]

[a]*School of Civil Engineering, College of Engineering, University of Tehran, 14155-6619 Tehran, Iran, Tel. +98-21-61112237; email: snazif@ut.ac.ir (S. Nazif)*
[b]*Department of Civil Engineering, Isfahan University of Technology, 84156 Isfahan, Iran*

Received 22 December 2020; Accepted 14 April 2021

ABSTRACT

Phenol is a harmful substance even at low concentrations. The photocatalytic process is a suitable method for phenol treatment due to its characteristics. The complexity of the photocatalytic reactions is one of the problems for the applicability of photocatalytic technology in large-scale wastewater treatment. The data mining approach is a suitable solution for this problem. In this study, artificial neural network (ANN) and random forest (RF) methods were used to predict the efficiency of phenol removal using the data obtained from a cascade photocatalytic backlight reactor with TiO_2 as photocatalyst. The effect of operational parameters, that is, TiO_2 concentration 40–100 g/m^2, initial phenol concentration 50–700 mg/L, and pH 8, 9 was investigated and kinetic of phenol degradation was determined. On the ANN model using 15 neurons in the hidden layer allowed to obtain the best values for R^2 and MSE as 0.9996 and 0.36 mg/L, respectively, and on the RF model, the best values for R^2 and the MSE were 0.9972 and 1.36 mg/L, respectively. Comparing model outputs with lab results showed RF and ANN can be used for predicting phenol photocatalytic degradation with satisfying accuracy.

Keywords: Neural network; Random forest; Controlled random search; Titania nanoparticles; Phenol degradation; Photocatalytic reactor; Data mining

1. Introduction

Wastewater originated by industrial activities contains a variety of hazardous materials that may pollute air and water and result in harmful effects on both ecosystems and humans. Phenol is one of these materials and it can be found in various industrial wastewaters like an olive mill, and petrochemical factories [1]. It is a toxic and organic aromatic compound (C_6H_5OH) consisting of a phenyl group ($–C_6H_5$) which bonded to a hydroxyl group (–OH) [2]. In addition to natural sources of phenol production, the release of phenol-containing industrial wastewater in the environment has increased phenol supply in water resources. Phenolic compounds can create complexes with chlorine which cause an unpleasant taste and odor in water [3]. Phenol has harmful effects on human health. It can be absorbed from the skin rapidly and it can be bio-accumulated. Also, it can cause eye and skin burns in case of contact. Based on Environmental Protection Agency (EPA) classification, phenolic compounds are classified as the main pollutants and they are suspected to cause cancer and harm fetus [4–6]. Due to its harmful effects on health, various regulatory authorities have imposed strict limits to phenol concentration in industrial discharges and drinking waters. Based on the guidelines prescribed by WHO, a concentration of 1 μg/L phenol is allowed for drinking water. EPA has declared that the concentration of phenol in lakes and streams should be limited to 0.3 mg/L [7]. Therefore, removing phenol and its derivatives from water and wastewaters considered essential. For this purpose, various methods have been used such as biological treatment [8], electrochemistry [9], absorption [10],

* Corresponding author.

halloysite-based adsorbent [11], bio-filter [12], and cavitation [13]. The advanced oxidation process (AOP) is one of the most effective ways for the treatment of organic pollutants from water and wastewater [14,15]. In compression to conventional methods AOP has several benefits such as (1) it is capable of complete mineralization of organic materials, (2) it produces no sludge, (3) the energy consumption is low [16]. In the AOP methods generated hydroxyl and super anion radicals are responsible for organic pollutant degradation.

Heterogeneous photocatalysis is an AOP method and has been reported to treat organic pollutants very effectively [17,18]. Several materials are investigated as a semiconductor in heterogeneous photocatalysis. TiO_2 is a semiconductor metal and because of having characteristics such as: being inactive, low price, stability, and having a large bandgap is the most favorite catalyst material in heterogeneous photocatalysis [19]. When TiO_2 is irradiated with ultraviolet (UV) light, it excites electrons in the valance band so that they are transferred to the conduction band and, as a result, holes are created in the valance band. These holes react with hydroxide ions and produce hydroxyl radicals [20]. Anatase, rutile, and brokit are three phases of TiO_2. Anatase and rutile are the most used types. Anatae band gap is around 3.1 ev and for rutile, it is 3.01 ev. Generally using two different semiconductors or using two phases of a semiconductor can lower the recombination rate of electron–hole and thus causes an increase in the degradation rate of organic matters [21]. Wastewater treatment using a heterogeneous photocatalytic process is done in two ways: (1) reactors with suspended photocatalyst, (2) reactors with fixed photocatalyst on a surface [22]. Suspended photocatalytic systems need an additional separation unit which raises the cost of treatment [23]. Hence, the fixed bed photocatalytic reactors have extensively attracted the attention of scientists to enhance the applicability of heterogeneous photocatalytic technology in large-scale water treatment [24]. Because many parameters influence the AOP reactions, modeling photocatalytic degradation using conventional mathematical modeling is too hard [25,26]. Data mining approaches like artificial neural networks (ANN) [27], support vector machines (SVMs) [25], adaptive neuro-fuzzy inference systems (ANFIS) [28] are suitable and efficient solutions for this problem.

ANN can identify the complex relationships between input and output variables with high efficiency and acceptable accuracy [29]. It has shown satisfactory performance in many areas of science and engineering. Recently, some researches have been performed using ANN in modeling heterogeneous photocatalysis process. Ghanbary et al. [30] prepared TiO_2 nanoparticles using the sol–gel method under different thermal conditions and predicted photocatalytic activity by ANN. Behnajady and Eskandarloo [31] prepared TiO_2 nanoparticles using the sol–gel method under different pH conditions and predicted the photocatalytic activity by ANN. Amani-Ghadim and Dorraji [32] investigated the photocatalytic activity of ZnO nanoparticles under different operational parameters and created a model using ANN.

Random forest (RF) is another data mining method which is introduced by Breiman [33]. It is a nonlinear method and can be used for classification and regression problems. Its application and accuracy in various filed of sciences are studied by various researchers and it was promising. Singh et al. [34] used the random forest to model the infiltration rate of soil and predicted the impact of water quality on it using the developed model. Hamidi et al. [35] investigated the application of the random forest method to predict snowfall. Naghibi et al. [36] used the random forest method to produce groundwater spring potential maps.

In this study, two models were created using RF and ANN methods for predicting the photocatalytic removal of phenol using the results obtained from a novel cascade catalytic reactor. The RF model has not been used in literature for this purpose. In addition, as a new approach, the optimal values of effective parameters in phenol removal (TiO_2 concentration, pH, initial phenol concentration, and treatment time) were obtained using controlled random search with local mutation algorithm and compared with lab results.

2. Materials and methods

2.1. Materials

In this empirical study, Tecnan Spain was used as a TiO_2 provider. The average size of TiO_2 particles used was 10–15 nm and its bandgap is 3.37 ev [37]. The amount of TiO_2 phases is 85% anatase and 15% rutile [38]. Phenol (purity over 99%), for adjusting pH, NaOH, and HCl of analytical reagent grade from Merck Co., (Germany) were used. For creating synthetic wastewater, phenol was dissolved in deionized water and for UV irradiation, 160 w Narva Black Light was used.

2.2. Cascade backlight photocatalytic reactor

In this study, the reactor was made up of three plexiglass rectangular reservoirs. The dimension of the plate at the bottom of the reservoir was 420 mm × 250 mm × 2 mm and the height of the edges was 4 cm and the weir was 2 cm. For phenol treatment, the synthetic wastewater was circulated in the reactor with a flow rate of 4 L/min, and to increase dissolved oxygen concentration an aerator was used. Each time the experiments were carried out to establish balance, while ultra-violet lamps were off, the synthetic wastewater was rotated in the reactor for 15 min. The sampling was performed every half hour and the total time of each test was 3 h. Fig. 1 shows the reactor used in this study.

2.3. Analysis method

4-aminoantipyrine colorimetric method was used to measure phenol concentration [39] and Hach Dr 2800 spectrophotometer was used for this purpose. For measuring pH OHAUS ST20 pH meter was used. For calculating the remaining phenol concentration Eq. (1) was used:

$$\text{Remaining phenol concentration} = \frac{C}{C_0} \times 100 \quad (1)$$

where C and C_0 are phenol and initial phenol concentration, respectively.

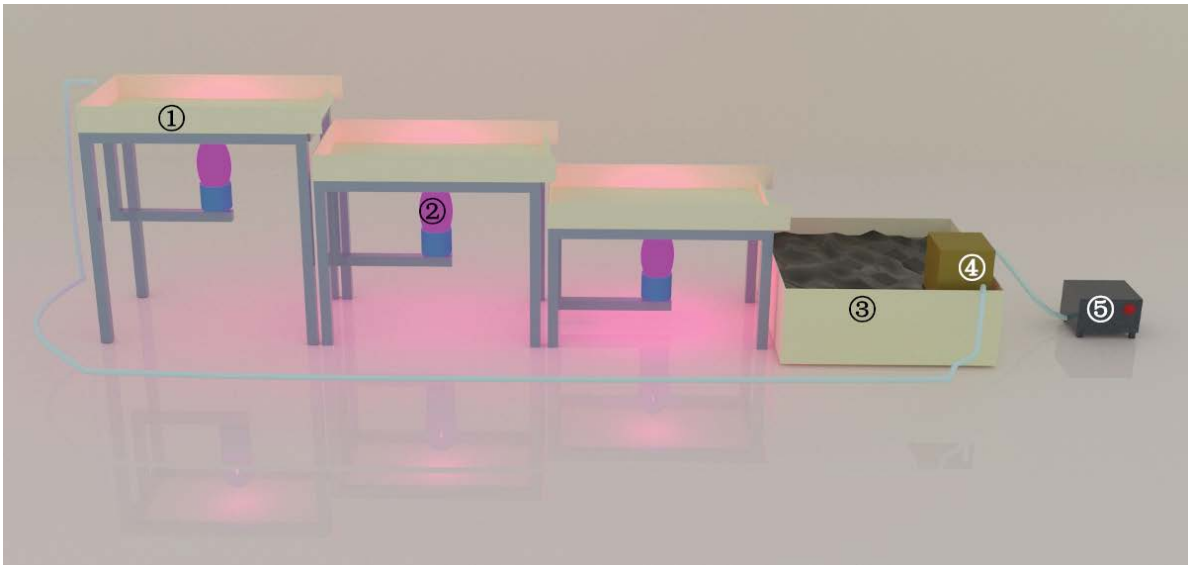

Fig. 1. Diagram of reactor used in this study.

2.4. Artificial neural networks

An ANN is an idea for information processing that is inspired by the biological nervous system and tries to process the information like the brain. The key element of this idea is the new structure of the information processing system. The system consists of a large number of interconnected processing elements called neurons that work together to solve a problem [40]. In this study, a three-layer perceptron ANN model including an input layer, hidden layer, and output layer was created. The input layer had four operational parameters (inputs) including treatment time, TiO_2 concentration, phenol initial concentration, and pH. For creating the best ANN model, tangent sigmoid (tansig), and log sigmoid (logsig) were examined for the hidden layer transfer function. The dependent variable of the output layer was the remaining phenol concentration and its transfer function was linear (purelin). Levenberg–Marquardt backpropagation algorithm was used for training the neural network and MATLAB version 9.1 (R2016b) was employed for processing data and creating ANN model. Fig. 2 shows the schematic architecture of the ANN model that was used in this study.

As mentioned tansig and logsig transfer functions were examined as hidden layer activation functions. Therefore, it was necessary to scale all input data but in the RF method, input data doesn't need to be scaled for model creation and therefore its output is not scaled too. Therefore, the ANN model was created in such a way that the input data were first scaled to the range –1 to 1 and after determining the result, it was again reverse-processed to its original state. In this way, it was possible to compare the outputs of the two methods.

2.5. Random forest

RF is an ensemble machine-learning algorithm introduced by Breiman [33]. It applies a combination of Bootstrap aggregating (bagging) and random variable selection techniques to the decision tree method and both regression and classification problems can be solved by it. RF uses a large number of decision trees, feeds each tree with a random sample with replacement from the main training data set, and chooses a subset of independent factors randomly at each node of a decision tree. Also, it should be noted that trees do not prune in an RF model [36]. This method decreases the correlation between individual trees and therefore increases the accuracy of the model. Almost only two-thirds of the training data appears in a bootstrap sample. One-third of the remainder, which is referred to as "out of bag sample (OOB sample)", is used to validate the model. This is done by calculating out-of-bag error (OOB error). In classification problems, one can well estimate the accuracy of a model using the OOB error value, but it is an approximation in regression problems [41]. In regression problems, the result will be determined by averaging the outcome of each tree. Like ANN, input parameters were treatment time, TiO_2 concentration, phenol initial concentration, and pH. The remaining phenol concentration prediction was the output of the model. For creating the RF model in MATLAB software, RF-Matlab

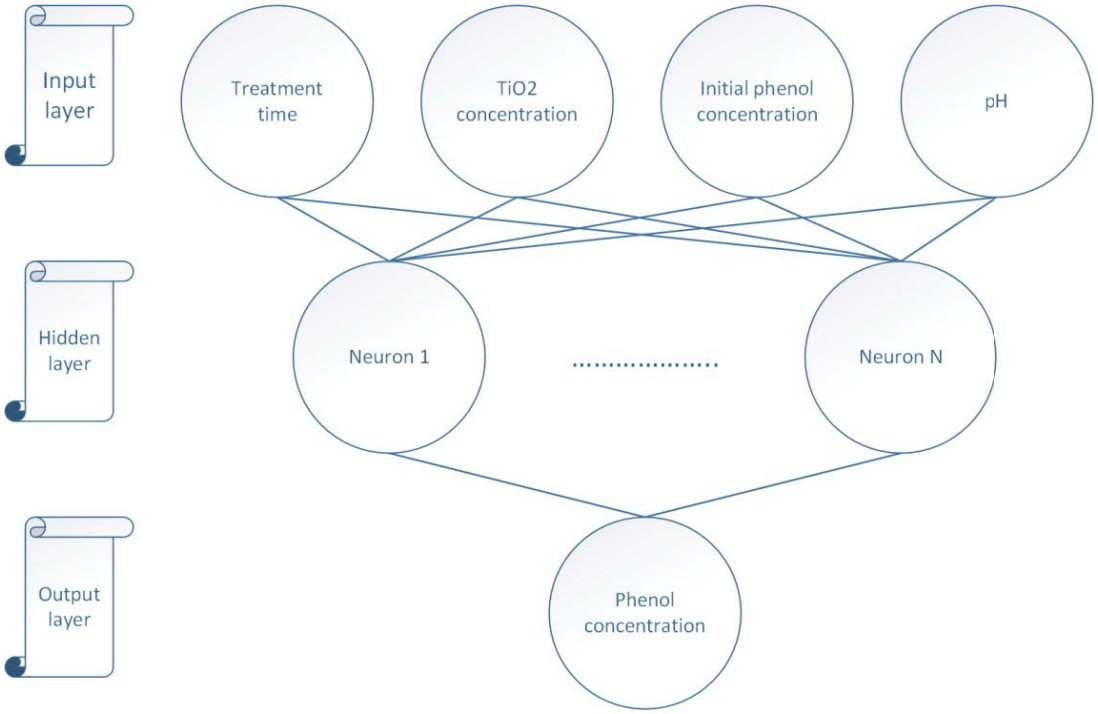

Fig. 2. Schematic diagram of the proposed ANN model.

package written by Jaiantilal, A. (n.d.) was used and it can be downloaded from https://github.com/jrderuiter/randomforest-matlab. This package uses the classification and regression trees (CART) algorithm for building decision trees. Fig. 3 shows the schematic diagram of the random forest model used in this study.

The following parameters were used to determine the best architecture of the RF model: n_{tree}, the number of decision trees; m_{try}, number of independent variables which can be selected randomly; node size, which minimum size of terminal nodes is determined by this parameter. Using larger values for node size causes smaller trees to be grown.

2.6. Reactor parameters optimization

Data mining models also can be used to optimize system parameters. For this purpose, the global optimization algorithm called controlled random search with local mutation (CRS) was used [42]. It was first introduced by Price in 1978 [43]. NLOPT library has implemented this algorithm for MATLAB and was used in this study [44]. In this method, which is sometimes compared with a genetic algorithm, the problem should be boundary constrained and the optimization procedure starts with a population of points with random values where these points randomly evolve using heuristic rules. In other words, the point with the worst value is replaced with a new point with a better value and this loop continues until a certain condition is met [45].

3. Experiments

In this study, the effect of phenol concentration, pH, and TiO_2 concentration were investigated. The full factorial method was used for designing experiments. Table 1 shows parameters considered in this study and their ranges. Initial phenol concentration and pH ranges were selected based on petrochemical wastewater characteristics and TiO_2 concentration was chosen based on the previous studies.

Input variable for ANN and RF models are treatment time (min), initial pH, initial phenol concentration (mg/L), and TiO_2 concentration (g/m^2). The remaining phenol concentration was chosen as the target variable. In this study, 192 samples were used to feed the ANN and RF models.

4. Results and discussion

4.1. Kinetics of phenol photocatalytic degradation

In general, photocatalytic reactions follow first-order kinetics [52]. Kinetics of photocatalytic oxidation of phenol is also pseudo-first-order [51]:

$$r = \frac{-dc}{dt} = kc \tag{2}$$

where k (min^{-1}) is the rate constant. By integrating Eq. (2) and considering the initial concentration of phenol equal to C_0, the following equation is derived:

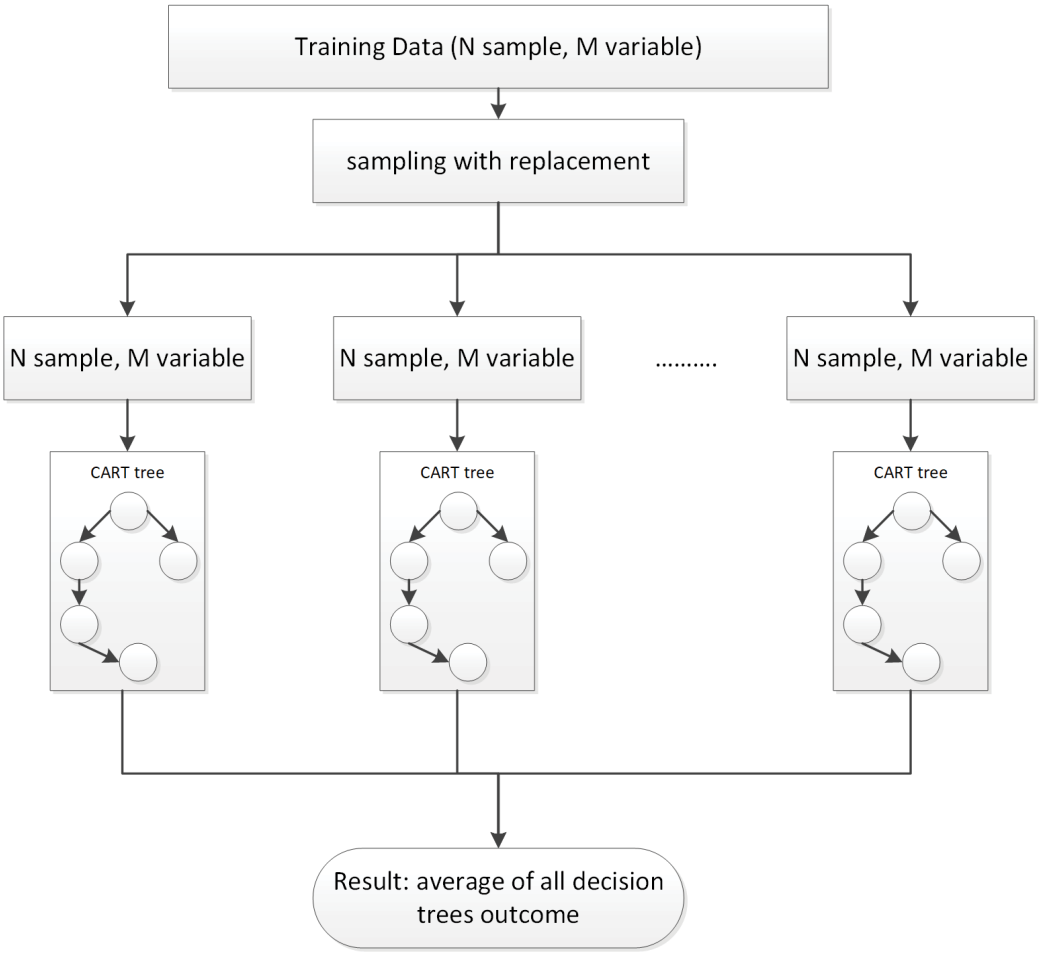

Fig. 3. Schematic diagram of the RF model.

Table 1
Selected experiment parameters

Parameter	Values	References
Time, min	30, 60, 90, 120, 150, 180	
pH	8, 9	[46–48]
Phenol, mg/L	50, 250, 500, 700	[49,50]
TiO_2, g/m^2	40, 60, 80, 100	[51]

$$\ln\left(\frac{C}{C_0}\right) = -kt \tag{3}$$

where C is phenol concentration at time t (min). To calculate k, first $-\ln(C/C_0)$ was plotted against t, then linear regression analysis was used. The slope of the resulting linear regression model is equal to k. The results of linear regression analysis confirmed that the photocatalytic oxidation of phenol in experiments follows pseudo-first-order kinetics.

Table 2
Correlation coefficient (R^2) and rate constant (k) for phenol removal with pH = 8

TiO_2 concentration (g/m^2)	Initial phenol concentration (mg/L)					
	50		100		500	
	k	R^2	k	R^2	k	R^2
40	0.0044	0.95	0.0035	0.93	0.0019	0.94
60	0.0049	0.97	0.0045	0.98	0.0028	0.97
80	0.0098	0.99	0.0091	0.97	0.0055	0.99
100	0.0107	0.98	0.0098	0.99	0.0058	0.98

4.1.1. Effect of TiO_2 and initial phenol concentration in k

Table 2 shows changes in the k relative to the TiO_2 and initial phenol concentration. The results showed that with increasing TiO_2 concentration, the amount of k also increases. Hydroxyl radical produced in photocatalytic reactions is the main cause of photocatalytic oxidation of phenol [20]. Hence, as the concentration of TiO_2 increased,

the rate of hydroxyl radical production also increased and the oxidation rate of phenol increased too. The results showed that with increasing initial phenol concentration, the amount of *k* decreased. This is because that photocatalytic oxidation occurs on the surface of TiO_2 particles and there is a limited number of oxidation sites [51].

4.1.2. Effect of pH changes in k

Table 3 shows the effect of pH changes in the variation of *k*. The results showed that by changing pH from 8 to 9, the amount of *k* increased. Increasing pH increases the production of hydroxyl radicals [38] and thus increases the value of *k*.

4.2. ANN model

For developing the model, the data were divided into training data (70%), validating data (15%), and testing data (15%). Also, mean squared error (MSE) and coefficient of determination (R^2) were used to evaluate the model accuracy. MSE value is calculated using Eq. (4):

$$\mathrm{MSE} = \frac{1}{N}\sum_{i=1}^{N}\left(y_{\mathrm{prd},i} - y_{\mathrm{exp},i}\right)^2 \tag{4}$$

and R^2 value is calculated using Eq. (5):

$$R^2 = 1 - \left(\frac{\sum_{i=1}^{N}\left(y_{\mathrm{prd},i} - y_{\mathrm{exp},i}\right)^2}{\sum_{i=1}^{N}\left(y_{\mathrm{exp},i} - y_m\right)^2}\right) \tag{5}$$

Table 3
Correlation coefficient (R^2) and rate constant (*k*) for phenol removal with TiO_2 = 60 g/m²

Initial phenol concentration (mg/L)	pH			
	8		9	
	k	R^2	*k*	R^2
50	0.0049	0.97	0.0052	0.95
100	0.0045	0.98	0.0049	0.96
500	0.0028	0.97	0.0034	0.99

where $y_{\mathrm{prd},i}$ and $y_{\mathrm{exp},i}$ are predicted and lab result of remaining phenol concentration respectively, and y_m is the average of the lab results. The number of neurons in the hidden layer is an effective factor for creating an accurate model. This parameter should be selected in such a way that, the value of R^2 is maximized and the amount of MSE is minimized. To achieve the best accuracy, a range of 1–21 for neurons in the hidden layer was examined. Table 4 shows calculated MSE and R^2 indices for the different number of neurons in the hidden layer.

As Table 4 shows that the best result was R^2 = 0.9996 and MSE = 0.36 and it was achieved when 15 neurons were used in the hidden layer. Table 5 shows ranges of considered parameters in building the ANN model for predicting remaining phenol concentration and the selected values based on the performance criteria of R^2 and MSE.

Fig. 4 shows MSE value vs. training epochs of model training for the selected ANN model. As it can be seen training was stopped after 38 epochs.

The simulated and observed values in training, validation, and test samples, as well as all data, are compared in scatter plots provided in Fig. 5. As it can be seen the predicted values of C/C_0 completely follow the observed values as they fit the 45° line.

Other researchers achieved similar accuracy when using ANN method to predict TiO_2 photocatalytic behavior. For example, Lenzi et al. [53] used the ANN method to predict the photocatalytic degradation of textile reactive dye. The R^2 value of their optimized model was 0.9995. Bennemla et al. [26] used the ANN method to predict photocatalytic

Table 5
Considered parameters for ANN model creation, examined range, and the selected values

Parameter	Value	Examined range
Neurons in input layer	4	–
Neurons in hidden layer	15	1–21
Neurons in output layer	1	–
Training function	Levenberg–Marquardt	–
Hidden layer function	tansig	logsig–tansig
Output layer function	purlin	–

Table 4
MSE and R^2 indices for different number of neurons in the hidden layer

Hidden layer size	R^2	MSE (mg/L)	Hidden layer size	R^2	MSE (mg/L)	Hidden layer size	R^2	MSE (mg/L)
1	0.931	66.27	9	0.9991	0.88	17	0.9995	0.51
2	0.9644	34.83	10	0.999	0.97	18	0.9995	0.51
3	0.9854	14.36	11	0.9993	0.73	19	0.9996	0.4
4	0.9931	6.89	12	0.9993	0.66	20	0.9992	0.81
5	0.9953	4.72	13	0.9995	0.53	21	0.9994	0.59
6	0.998	2	14	0.9993	0.73			
7	0.9984	1.55	15	0.9996	0.36			
8	0.9982	1.8	16	0.9994	0.57			

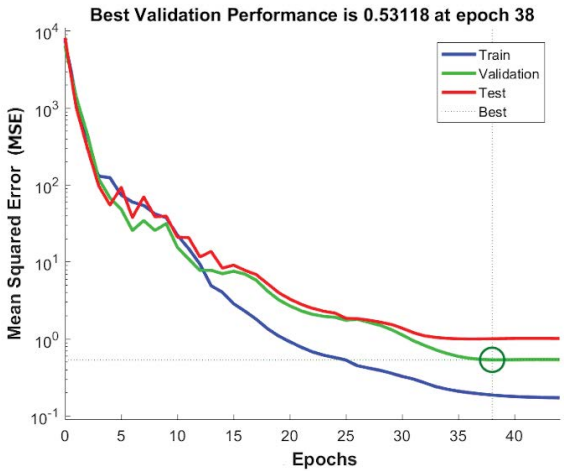

Fig. 4. MSE vs. the number of epochs.

degradation of oxytetracycline. The R^2 value of the created model was 0.9975. Hence, ANN is a reliable method to predict TiO_2 photocatalytic degradation.

4.3. RF model

Because OOB error is used for validating the RF model, there was no need for separate validating data set. Therefore the experimental data set was randomly divided into 163 samples for train data (85%) and 29 samples for test data (15%). As mentioned, RF is a collection of decision trees. For modeling with a decision tree, there is no need for data scaling, hence RF does not require data normalization too. Like the ANN model, MSE and R^2 indices were used to evaluate model accuracy [Eqs. (4) and (5)]. Table 6 shows the considered ranges of RF model parameters and selected tuning parameters of the model for predicting remaining phenol concentration in wastewater.

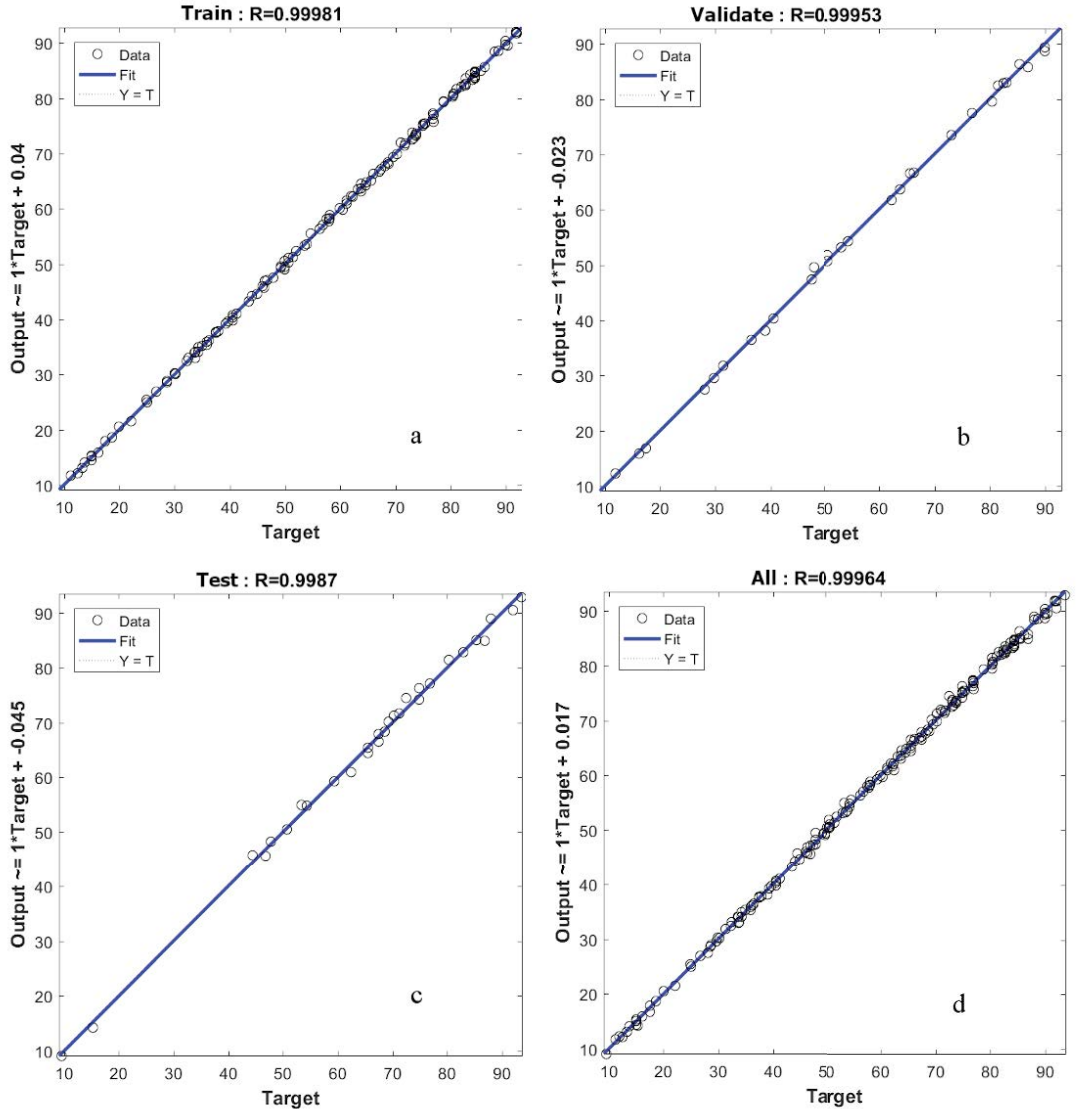

Fig. 5. ANN model regression diagrams: (a) train data, (b) validate data, (c) test data, and (d) all data.

Table 6
Examined RF parameters

Parameter	Selected value	Examined range
n_{tree}	200	Up to 1,000
m_{try}	4	1–4
Node size	3	1–5

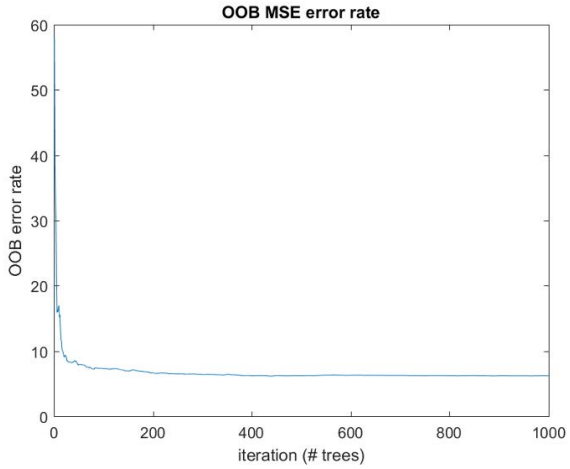

Fig. 6. OOB error rate vs. number of trees.

Fig. 6 shows the OOB error rate vs. number of trees. As it shows in 200 trees, the OOB error rate converges and the model with 200 trees produced the best results.

MSE value of the selected RF model was 1.36 and the R^2 value was 0.9972. The convergence between model outputs and observed values shown in Fig. 7.

4.4. Initial phenol concentration effect

To study the effect of initial phenol concentration in phenol removal efficiency, initial phenol concentration from 50 to 700 mg/L is investigated. Results showed that an increment in initial phenol concentration causes a decrement in phenol removal efficiency. For example, when TiO_2 concentration equals 40 g/m^2, phenol removal efficiency decreased from 66% to 36% when phenol initial concentration increased from 50 to 700 mg/L. Fig. 8 shows experimental results and predicted values by the selected ANN and RF models.

4.5. Initial pH effect

pH is an important factor in photocatalytic treatment because the ionization status of both photocatalyst and target substance surface are pH-dependent. In this study, phenol removal performance was investigated in pH values of 8 and 9. Results showed that increment on initial pH causes increment on phenol removal efficiency. Fig.

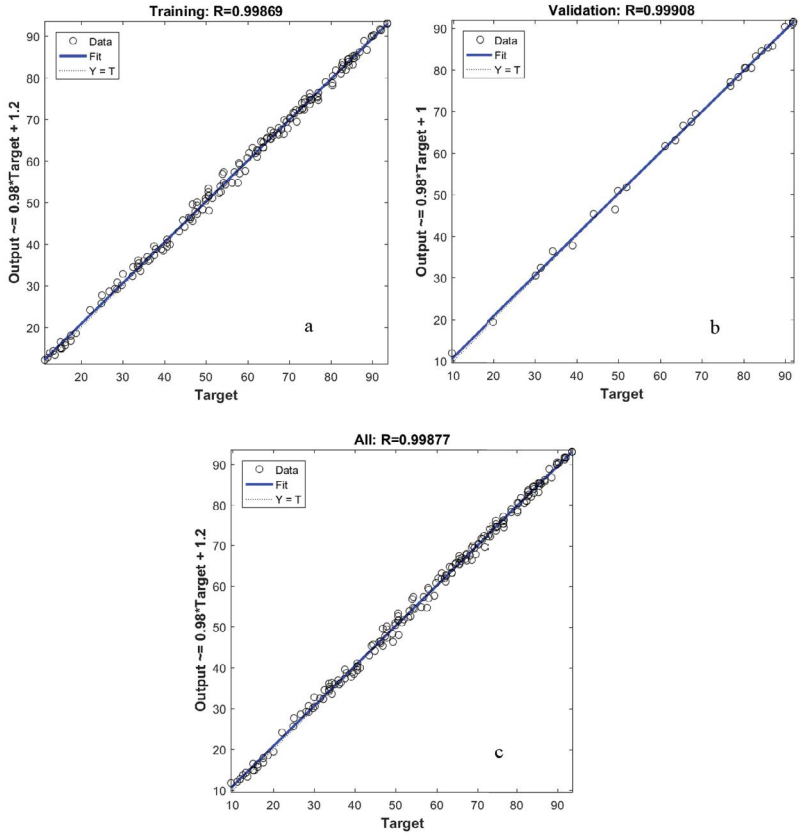

Fig. 7. RF model regression diagrams: (a) train data, (b) validate data, and (c) all data.

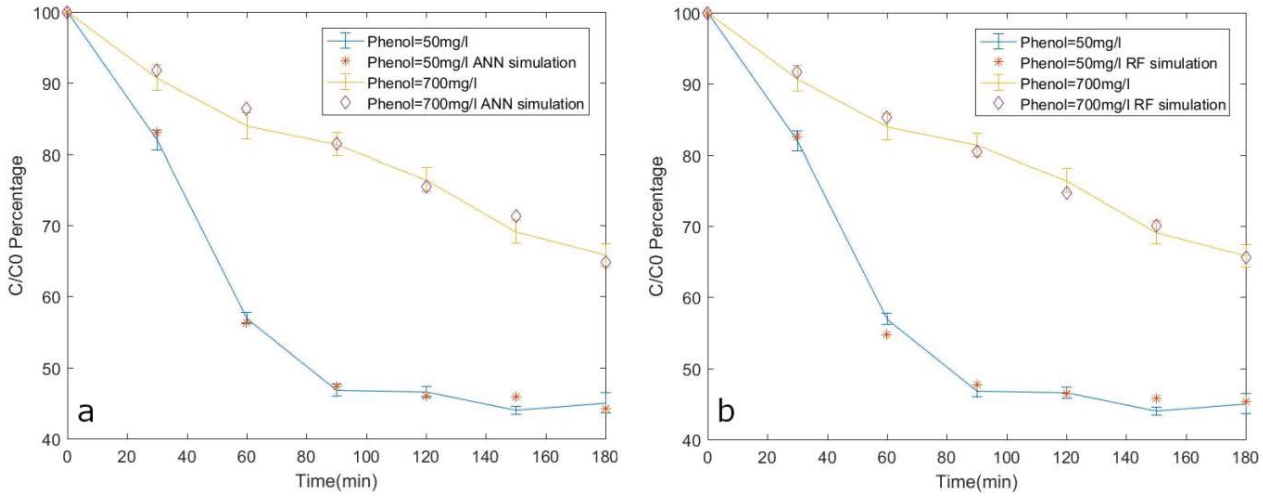

Fig. 8. Photocatalytic degradation of phenol with TiO_2 = 40 g/m², pH = 9, and comparison with optimized model output (error bars represent standard deviation among duplicate tests): (a) ANN and (b) RF.

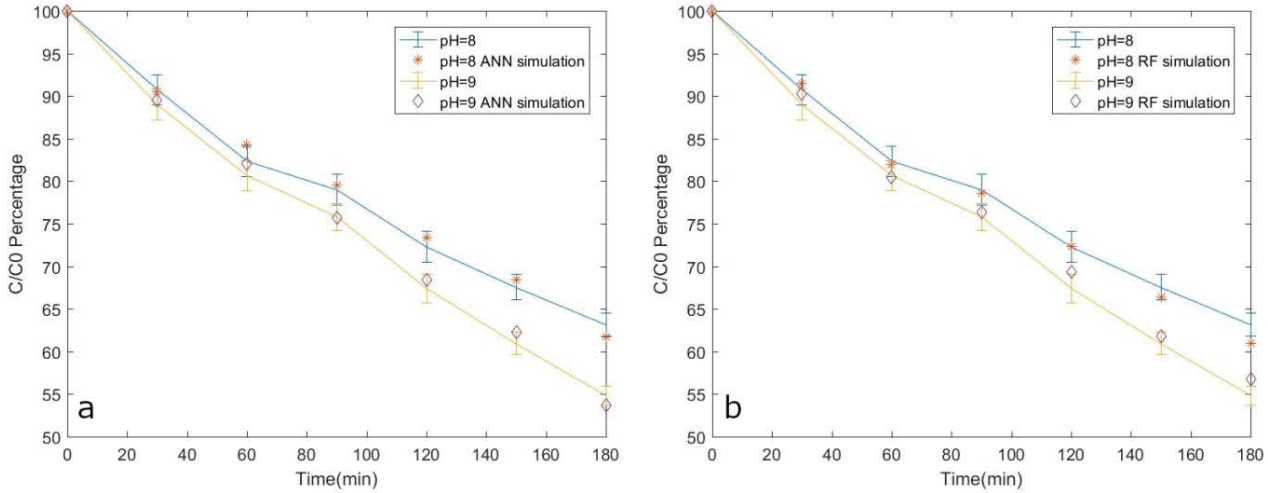

Fig. 9. Photocatalytic degradation of phenol with TiO_2 = 60 g/m², phenol = 700 mg/L, and comparison with optimized model output (error bars represent standard deviation among duplicate tests): (a) ANN and (b) RF.

9 shows the experimental result and predicted values by ANN and RF models with TiO_2 equals 60 g/m² and initial phenol equals 700 mg/L with pH 8 and 9.

4.6. TiO_2 concentration effect

Another variable that its effect on the phenol removal efficiency was investigated is TiO_2 concentration. Based on the test results, with an increase in TiO_2 concentration until 80 g/m², phenol treatment efficiency also increased and it could be due to the increase in the surface available for the photocatalytic reaction. Increasing the surface area causes charge carriers concentration increment and therefore causes an increase in hydroxyl radicals generation [26]. For example with initial phenol concentration equals 700 mg/L and pH equals 9, the phenol removal efficiency increased from 36% to 69% after 180 min treatment when TiO_2 concentration increased from 40 to 80 g/m², respectively. However, TiO_2 concentration increase from 80 to 100 g/m² did not highly affect phenol removal efficiency. Lack of space for TiO_2 nanoparticles and surface saturation can cause this problem. Fig. 10 shows experimental results and predicted values by ANN and RF models when pH, initial phenol concentration, and TiO_2 concentration are equal to 8, 700 mg/L, and 40 and 80 g/m², respectively.

4.7. Optimizing reactor parameters using ANN and RF models

Two developed models were used to determine the best operational parameters of the reactor using the CRS

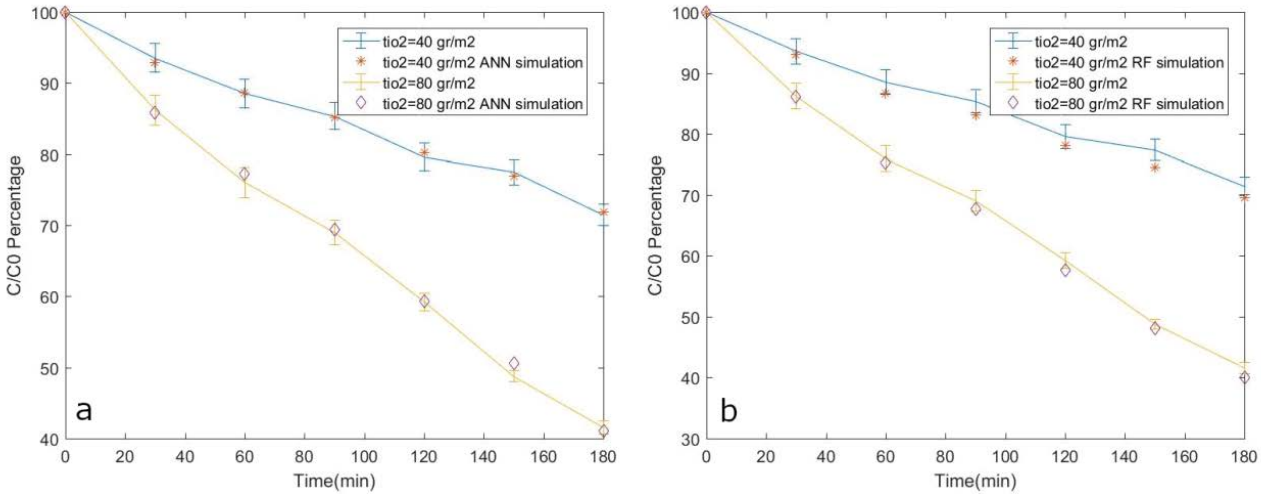

Fig. 10. Photocatalytic degradation of phenol with phenol = 700 mg/L, pH = 8, and comparison with optimized model output (error bars represent standard deviation among duplicate tests): (a) ANN and (b) RF.

Table 7
Best values of MSE and R^2 indices for ANN and RF methods

	ANN	RF	Lab
Initial phenol concentration (mg/L)	50	50	50
TiO_2 concentration (g/m^2)	91.5	90.56	100
pH	9	9	9
Treatment time (min)	180	180	180
Remaining phenol concentration (%)	8.16	10.1	9.6

Table 8
Removal efficiencies of other treatment methods for petrochemical and oil refinery wastewater

Method	Treatment time (min)	Initial phenol concentration (mg/L)	Removal efficiency (%)	Study
Photocatalytic degradation (ZnO/TiO_2)	160	60	100	[54]
Sono-photo-Fenton	60	50	76.1	[55]
Biochar-La/ultrasonic/persulfate	63	86	97.68	[56]
Electroflotation/electrocoagulation	30	3.17	65	[57]
Biodegradation using bacteria strain *Acinetobacter calcoaceticus*	2,880	800	91.6	[58]
Anaerobic stabilization pond	2,880	200	81.63	[5]

Table 9
Best values of MSE and R^2 indices for ANN and RF methods

Method	MSE	R^2
ANN	0.36	0.9996
RF	1.36	0.9972

algorithm. In NLOPT implantation of CRS, the default value for initial population size is $10 \times (n + 1)$ where n is the number of variables we need to optimize. In this study, the default value is used and three variables of initial phenol concentration, TiO_2 concentration, and pH were optimized. As mentioned in section 2.6 (Reactor parameters optimization), in CRS the upper and lower limit of optimization variables must be determined. Thus initial phenol concentration 50 and 700, pH 8 and 9, and TiO_2 concentration 40 and 100 were used as the lower and upper limits, respectively. Table 7 shows optimized reactor parameters and predicted remaining phenol concentration after 180 min treatment. For comparison, the best result obtained from lab experiments is also provided. As Table 7 shows, the results between developed simulation models and lab experiments are satisfactorily close and both models have adequate performance in this regard.

Table 10
Modeling methods used for predicting phenolic compounds photocatalytic degradation

Photocatalyst	Contaminant	Modeling method	Input variables	Output variable	Reference
SnO_2/Fe_3O_4	Phenol red	ANN	Phenol red, stirring intensity, and UV intensity	Removal (%)	[59]
TiO_2	4-nitrophenol	ANN	Nano TiO_2, time, UV intensity, 4-NP	Removal (%)	[30]
Ag/ZnO	Bisphenol-A	ANN	Ag/ZnO, pH, initial bisphenol-A concentration, light wavelength, reaction time	Degradation rate	[60]
TiO_2	4-Chlorophenol	ANN/RSM	Initial 4-chlorophenol concentration, TiO_2, pH	Removal (%)	[61]
TiO_2	Phenol	RSM	Phenol concentration, catalyst doses, and degradation time	Removal (%)	[62]
TiO_2	Phenol	Box–Benkhen	TiO_2 size, TiO_2 concentration, dissolved oxygen concentration, and phenol concentration	Degradation rate	[63]
TiO_2	Phenol	Cubic model	UV irradiation intensity, pH	Degradation rate	[64]

As mentioned in section 3 (Experiments), the initial phenol concentration and pH ranges used in this study are based on petrochemical wastewater characteristics. Other studies used different methods for the treatment of phenol in petrochemical wastewater. Some of these methods and their removal efficiencies are shown in Table 8. Comparing the removal efficiency from this study and Table 8 shows that the results are in the range of other studies and phenol treatment efficiency is satisfactory.

4.8. Comparison of ANN and RF models

The performance of created models is summarized in Table 9. As seen in Figs. 5 and 7 and also Table 7, the trend of C/C_0 in created RF and ANN models fit the 45° line in a satisfactory manner. Hence, both models have acceptable accuracy for predicting phenol treatment efficiency. As seen in Table 8, it can be concluded that the ANN method is a little more accurate than RF.

In other studies, modeling the photocatalytic degradation of phenol is not limited to ANN and in addition to phenol, these methods have been used for modeling other phenolic compounds photocatalytic degradation too. Table 10 summarizes some of these studies.

5. Conclusion

In this research, photocatalytic treatment of phenol using a photocatalytic backlight reactor has been investigated. The results showed that the phenol degradation process follows pseudo-first-order kinetics. Changes in k with changes in operational parameters showed that as pH and TiO_2 increased, the phenol removal efficiency increased too and with initial phenol concentration increase, phenol removal efficiency decreased. The impact of operational parameters on phenol removal efficiency has been modeled using ANN and RF methods. For the ANN model, a three-layer perceptron with 15 neurons in the hidden layer has been used. MSE and R^2 values for this model were 0.36 mg/L and 0.9996, respectively. RF model has been created using 200 trees and MSE and R^2 values for this model were 1.36 mg/L and 0.9972, respectively. CRS algorithm has been used to optimize operational parameters with RF and ANN models. Comparing obtained results and lab data showed both ANN and RF can predict phenol removal with satisfying accuracy. It is suggested to investigate COD reduction and mineralization by COD and TOC tests, monitoring phenol solution degradation by UV/Vis spectrum test, and identification of intermediates in the degradation of phenol by HPLC/MS or GC/MS in future studies.

References

[1] S. Mohammadi, A. Kargari, H. Sanaeepur, K. Abbassian, A. Najafi, E. Mofarrah, Phenol removal from industrial wastewaters: a short review, Desal. Water Treat., 53 (2015) 2215–2234.
[2] Z. Rappoport, The Chemistry of Phenols, Vol. 2, Set John Wiley & Sons, West Sussex, England, 2004.

[3] A. Almasi, M. Mahmoudi, M. Mohammadi, A. Dargahi, H. Biglari, Optimizing biological treatment of petroleum industry wastewater in a facultative stabilization pond for simultaneous removal of carbon and phenol, Toxin Rev., 38 (2019) 1–9, doi: 10.1080/15569543.2019.1573433.
[4] A. Almasi, A. Dargahi, A. Amrane, M. Fazlzadeh, M. Soltanian, A. Hashemian, Effect of molasses addition as biodegradable material on phenol removal under anaerobic conditions, Environ. Eng. Manage. J., 17 (2018) 1475–1482.
[5] A. Dargahi, M. Mohammadi, F. Amirian, A. Karami, A. Almasi, Phenol removal from oil refinery wastewater using anaerobic stabilization pond modeling and process optimization using response surface methodology (RSM), Desal. Water Treat., 87 (2017) 199–208.
[6] R. Shokoohi, H. Movahedian, A. Dargahi, A.J. Jafari, A. Parvaresh, Survey on efficiency of BF/AS integrated biological system in phenol removal of wastewater, Desal. Water Treat., 82 (2017) 315–321.
[7] A.K. Rathoure, Toxicity and Waste Management Using Bioremediation, IGI global, Hershey PA, USA, 2015.
[8] E. Ferrer-Polonio, N.T. García-Quijano, J.A. Mendoza-Roca, A. Iborra-Clar, L. Pastor-Alcañiz, Effect of alternating anaerobic and aerobic phases on the performance of a SBR treating effluents with high salinity and phenols concentration, Biochem. Eng. J., 113 (2016) 57–65.
[9] X. Duan, F. Ma, Z. Yuan, L. Chang, X. Jin, Electrochemical degradation of phenol in aqueous solution using PbO_2 anode, J. Taiwan Inst. Chem. Eng., 44 (2013) 95–102.
[10] E. Lorenc-Grabowska, G. Gryglewicz, M.A. Diez, Kinetics and equilibrium study of phenol adsorption on nitrogen-enriched activated carbons, Fuel, 114 (2013) 235–243.
[11] I. Anastopoulos, A. Mittal, M. Usman, J. Mittal, G. Yu, A. Núñez-Delgado, M. Kornaros, A review on halloysite-based adsorbents to remove pollutants in water and wastewater, J. Mol. Liq., 269 (2018) 855–868.
[12] R. Shokoohi, A.J. Jafari, A. Dargahi, Z. Torkshavand, Study of the efficiency of bio-filter and activated sludge (BF/AS) combined process in phenol removal from aqueous solution: determination of removing model according to response surface methodology (RSM), Desal. Water Treat., 77 (2017) 256–263.
[13] P.R. Gogate, Treatment of wastewater streams containing phenolic compounds using hybrid techniques based on cavitation: a review of the current status and the way forward, Ultrason. Sonochem., 15 (2008) 1–15.
[14] R. Shokoohi, R.A. Gillani, M.M. Mahmoudi, A. Dargahi, Investigation of the efficiency of heterogeneous Fenton-like process using modified magnetic nanoparticles with sodium alginate in removing Bisphenol A from aquatic environments: kinetic studies, Desal. Water Treat., 101 (2018) 185–192.
[15] A. Almasi, A. Dargahi, M. Mohammadi, A. Azizi, A. Karami, F. Baniamerian, Z. Saeidimoghadam, Application of response surface methodology on cefixime removal from aqueous solution by ultrasonic/photooxidation, Int. J. Pharm. Technol., 8 (2016) 16728–16736.
[16] V.K. Gupta, R. Jain, A. Mittal, T.A. Saleh, A. Nayak, S. Agarwal, S. Sikarwar, Photo-catalytic degradation of toxic dye amaranth on TiO_2/UV in aqueous suspensions, Mater. Sci. Eng., C, 32 (2012) 12–17.
[17] H. Mehrizadeh, A. Niaei, H.H. Tseng, D. Salari, A. Khataee, Synthesis of $ZnFe_2O_4$ nanoparticles for photocatalytic removal of toluene from gas phase in the annular reactor, J. Photochem. Photobiol., A, 332 (2017) 188–195.
[18] M.E. Borges, M. Sierra, E. Cuevas, R.D. García, P. Esparza, Photocatalysis with solar energy: sunlight-responsive photocatalyst based on TiO_2 loaded on a natural material for wastewater treatment, Sol. Energy, 135 (2016) 527–535.
[19] V.K. Gupta, R. Jain, A. Mittal, M. Mathur, S. Sikarwar, Photochemical degradation of the hazardous dye Safranin-T using TiO_2 catalyst, J. Colloid Interface Sci., 309 (2007) 464–469.
[20] R. Jain, M. Mathur, S. Sikarwar, A. Mittal, Removal of the hazardous dye rhodamine B through photocatalytic and adsorption treatments, J. Environ. Manage., 85 (2007) 956–964.
[21] R.J. Tayade, R.G. Kulkarni, R.V. Jasra, Photocatalytic degradation of aqueous nitrobenzene by nanocrystalline TiO_2, Ind. Eng. Chem. Res., 45 (2006) 922–927.
[22] M. Chong, B. Jin, C. Chow, C. Saint, Recent developments in photocatalytic water treatment technology: a review, Water Res., 44 (2010) 2997–3027.
[23] S.J. Royaee, M. Sohrabi, N. Fallah, A comprehensive study on wastewater treatment using photo-impinging streams reactor: continuous treatment, Korean J. Chem. Eng., 29 (2012) 1577–1584.
[24] L. Zeng, X. Guo, C. He, C. Duan, Metal-organic frameworks: versatile materials for heterogeneous photocatalysis, ACS Catal., 6 (2016) 7935–7947.
[25] M. Vaez, M. Omidkhah, S. Alijani, A.Z. Moghaddam, M. Sadrameli, N.G. Zanjani, Evaluation of photocatalytic activity of immobilized titania nanoparticles by support vector machine and artificial neural network, Can. J. Chem. Eng., 93 (2015) 1009–1016.
[26] M. Bennemla, M. Chabani, A. Amrane, Photocatalytic degradation of oxytetracycline in aqueous solutions with TiO_2 in suspension and prediction by artificial neural networks, Int. J. Chem. Kinet., 48 (2016) 464–473.
[27] S. Dutta, S.A. Parsons, C. Bhattacharjee, S. Bandhyopadhyay, S. Datta, Development of an artificial neural network model for adsorption and photocatalysis of reactive dye on TiO_2 surface, Expert Syst. Appl., 37 (2010) 8634–8638.
[28] A. Buthiyappan, A.A. Abdul Raman, M. Davoody, W.M.A.W. Daud, Parametric study and process evaluation of Fenton oxidation: application of sequential response surface methodology and adaptive neuro-fuzzy inference system computing technique, Chem. Eng. Commun., 204 (2017) 658–676.
[29] Y. Singh, A.S. Chauhan, Neural networks in data mining, J. Theor. Appl. Inf. Technol., 5 (2009) 37–42.
[30] F. Ghanbary, N. Modirshahla, M. Khosravi, M.A. Behnajady, Synthesis of TiO_2 nanoparticles in different thermal conditions and modeling its photocatalytic activity with artificial neural network, J. Environ. Sci., 24 (2012) 750–756.
[31] M.A. Behnajady, H. Eskandarloo, Preparation of TiO_2 nanoparticles by the sol–gel method under different pH conditions and modeling of photocatalytic activity by artificial neural network, Res. Chem. Intermed., 41 (2015) 2001–2017.
[32] A.R. Amani-Ghadim, M.S.S. Dorraji, Modeling of photocatalyatic process on synthesized ZnO nanoparticles: kinetic model development and artificial neural networks, Appl. Catal., B, 163 (2015) 539–546.
[33] L. Breiman, Random forests, Mach. Learn., 45 (2001) 5–32.
[34] B. Singh, P. Sihag, K. Singh, Modelling of impact of water quality on infiltration rate of soil by random forest regression, Model. Earth Syst. Environ., 3 (2017) 999–1004.
[35] O. Hamidi, L. Tapak, H. Abbasi, Z. Maryanaji, Application of random forest time series, support vector regression and multivariate adaptive regression splines models in prediction of snowfall (a case study of Alvand in the middle Zagros, Iran), Theor. Appl. Climatol., 134 (2018) 769–776.
[36] S.A. Naghibi, H.R. Pourghasemi, B. Dixon, GIS-based groundwater potential mapping using boosted regression tree, classification and regression tree, and random forest machine learning models in Iran, Environ. Monit. Assess., 188 (2016) 1–27.
[37] J.J. Reinosa, P. Leret, C.M. Álvarez-Docio, A. del Campo, J.F. Fernández, Enhancement of UV absorption behavior in ZnO–TiO_2 composites, Bol. Soc. Español. Cerámi. Vidr., 55 (2016) 55–62.
[38] A.M. Khaksar, S. Nazif, A. Taebi, E. Shahghasemi, Treatment of phenol in petrochemical wastewater considering turbidity factor by backlight cascade photocatalytic reactor, J. Photochem. Photobiol., A, 348 (2017) 161–167.
[39] APHA, WPCF, Standard Methods for the Examination of Water and Wastewater, Vol. 21, American Public Health Association/Water Pollution Control Federation, Washington DC, 2005.

[40] A.R. Khataee, M.B. Kasiri, Artificial neural networks modeling of contaminated water treatment processes by homogeneous and heterogeneous nanocatalysis, J. Mol. Catal. A: Chem., 331 (2010) 86–100.
[41] L. Breiman, Out-of-Bag Estimation, 1996. Available at: ftp.stat.berkeley.edu/pub/users/breiman/OOBestimation.ps
[42] D.P. Solomatine, Genetic and Other Global Optimization Algorithms-Comparison and Use in Calibration Problems, Proceedings of the 3rd International Conference on Hydroinformatics, Balkema, 1998, pp. 1–2.
[43] W.L. Price, A controlled random search procedure for global optimisation, Comput. J., 20 (1977) 367–370.
[44] S.G. Johnson, The NLopt Nonlinear-Optimization Package. Available at: http://github.com/stevengj/nlopt
[45] B. Kang, C. Sklibosios Nikitopoulos, E. Schlogl, B. Taruvinga, The Impact of Jumps on American Option Pricing: The S&P 100 Options Case, 2019.
[46] L. Fratila-Apachitei, Influence of membrane morphology on the flux decline during dead-end ultrafiltration of refinery and petrochemical waste water, J. Membr. Sci., 182 (2001) 151–159.
[47] T.H. Khaing, J. Li, Y. Li, N. Wai, F. Wong, Feasibility study on petrochemical wastewater treatment and reuse using a novel submerged membrane distillation bioreactor, Sep. Purif. Technol., 74 (2010) 138–143.
[48] N.M. Azeez, A.A. Sabbar, Efficiency of duckweed (*Lemna minor* L.) in phytotreatment of wastewater pollutants from Basrah oil refinery, J. Appl. Phytotechnol. Environ. Sanit., 1 (2012) 163–172.
[49] H. Oubrayme, S. Souabi, M. Bouhria, M. Tahiri, S.A. Younssi, A. Albizane, Performance of wastewater treatment in petrochemical refinery plant SAMIR, Int. J. Eng. Innovation Technol., 5 (2015) 74–81.
[50] S. Shanmugapriya, M. Premalatha, Solar photocatalytic treatment of phenolic wastewater potential, challenges and opportunites, J. Eng. Appl. Sci., 3 (2008) 36–41.
[51] M. Delnavaz, B. Ayati, H. Ganjidoust, S. Sanjabi, Kinetics study of photocatalytic process for treatment of phenolic wastewater by TiO_2 nano powder immobilized on concrete surfaces, Toxicol. Environ. Chem., 94 (2012) 1086–1098.
[52] Z. Khuzwayo, E.M.N. Chirwa, Analysis of catalyst photo-oxidation selectivity in the degradation of polyorganochlorinated pollutants in batch systems using UV and UV/TiO_2, South African, J. Chem. Eng., 23 (2017) 17–25.
[53] G.G. Lenzi, R.F. Evangelista, E.R. Duarte, L.M.S. Colpini, A.C. Fornari, R. Menechini Neto, L.M.M. Jorge, O.A.A. Santos, Photocatalytic degradation of textile reactive dye using artificial neural network modeling approach, Desal. Water Treat., 57 (2016) 14132–14144.
[54] F. Hayati, A.A. Isari, M. Fattahi, B. Anvaripour, S. Jorfi, Photocatalytic decontamination of phenol and petrochemical wastewater through ZnO/TiO_2 decorated on reduced graphene oxide nanocomposite: influential operating factors, mechanism, and electrical energy consumption, RSC Adv., 8 (2018) 40035–40053.
[55] A. Shokri, Application of sono-photo-Fenton process for degradation of phenol derivatives in petrochemical wastewater using full factorial design of experiment, Int. J. Ind. Chem., 9 (2018) 295–303.
[56] R. Razmi, B. Ramavandi, M. Ardjmand, A. Heydarinasab, Efficient phenol removal from petrochemical wastewater using biochar-La/ultrasonic/persulphate system: characteristics, reusability, and kinetic study, Environ. Technol., 40 (2019) 822–834.
[57] A. Dimoglo, H.Y. Akbulut, F. Cihan, M. Karpuzcu, Petrochemical wastewater treatment by means of clean electrochemical technologies, Clean Technol. Environ. Policy, 6 (2004) 288–295.
[58] Z. Liu, W. Xie, D. Li, Y. Peng, Z. Li, S. Liu, Biodegradation of phenol by bacteria strain *Acinetobacter calcoaceticus* PA isolated from phenolic wastewater, Int. J. Environ. Res. Public Health, 13 (2016) 300–308, doi: 10.3390/ijerph13030300.
[59] J. Sargolzaei, A. Hedayati Moghaddam, A. Nouri, J. Shayegan, Modeling the removal of phenol dyes using a photocatalytic reactor with SnO_2/Fe_3O_4 nanoparticles by intelligent system, J. Dispersion Sci. Technol., 36 (2015) 540–548.
[60] A.B. Jasso-Salcedo, S. Hoppe, F. Pla, V.A. Escobar-Barrios, M. Camargo, D. Meimaroglou, Modeling and optimization of a photocatalytic process: degradation of endocrine disruptor compounds by Ag/ZnO, Chem. Eng. Res. Des., 128 (2017) 174–191.
[61] P.S. Patel, V. Gandhi, M.P. Shah, T.S. Natarajan, K. Natarajan, R.J. Tayade, Modeling and optimization of photocatalytic degradation process of 4-chlorophenol using response surface methodology (RSM) and artificial neural network (ANN), Photocatalytic Nanomater. Environ. Appl., 27 (2018) 405.
[62] M. Zulfiqar, M.F.R. Samsudin, S. Sufian, Modelling and optimization of photocatalytic degradation of phenol via TiO_2 nanoparticles: an insight into response surface methodology and artificial neural network, J. Photochem. Photobiol., A, 384 (2019) 1–15, doi: 10.1016/j.jphotochem.2019.112039.
[63] S. Ray, J.A. Lalman, N. Biswas, Using the Box–Benkhen technique to statistically model phenol photocatalytic degradation by titanium dioxide nanoparticles, Chem. Eng. J., 150 (2009) 15–24.
[64] I. Udom, P.D. Myers, M.K. Ram, A.F. Hepp, E. Archibong, E.K. Stefanakos, D.Y. Goswami, Optimization of photocatalytic degradation of phenol using simple photocatalytic reactor, Am. J. Anal. Chem., 5 (2014) 743–750.